Journal of Al-Azhar University Engineering Sector

Vol. 19, No. 73, October 2024, 1369 - 1381

Challenges in Energy Savings in Aluminium Reduction Cell by Improving the Anode Design and Inserts

Abdul-Majid Shamroukh[1,*], Salah A. Salman [2], Amr B. ElDeeb[2], M. K. Gouda[2], W. Berends[3], W. Abdel-Fadeel[4], G.T. Abdel-Jaber[5]

[1] Aluminum Co. of Egypt (Egyptalum), Nag' Hammadi, 83642, Qena, Egypt

[2] Mining and Petroleum Department, Faculty of Engineering, Al-Azhar University, Nasr City, 11884, Cairo, Egypt,

[3]AluCellTech Inc. Canada.

[4] Mechanical Design and Production engineering, Faculty of Energy Engineering, Aswan University, 81542, Aswan, Egypt.

[5] Mechanical Design and Production Engineering, South Valley University, 83523, Qena, Egypt.

[*] **Correspondence**: abdulmajid_business@outlook.com

Citation:

A. Shamroukh, S. A. Salman, A. B. ElDeeb, M. K. Gouda, W. Berends, W. Abdel-Fadeel, G.T. Abdel-Jaber, " Challenges in Energy Savings in Aluminium Reduction Cell by Improving the Anode Design and Inserts", Journal of Al-Azhar University Engineering Sector, vol. 19, pp. 1369 - 1381, 2024.

Received: 29 May 2024

Revised: 28 August 2024

Accepted: 17 September 2024

Doi: 10.21608/auej.2024.249663.1481

ABSTRACT

The predominant method for primary aluminum production is the Hall-Héroult Electrolytic Process, which is marked by its high energy demands. The process's power efficiency poses a significant hurdle for aluminum producers, with values not exceeding 50%. Power consumption constitutes a substantial portion of the overall production cost, accounting for approximately 40%. The excessive electrical energy consumption stems primarily from the considerable voltage drop across both the anode and cathode. Notably, contact resistance is responsible for about 25% of the total voltage drop in the anode assembly, particularly at the interfaces between steel, cast iron, and carbon. A novel anode assembly design had been successfully developed and confirmed in-situ and numerically using various configurations of steel nails. A 3D thermo-electrical model of the anode assembly was constructed using the APDL language of ANSYS software. The 3D model was confirmed against a comprehensive set of temperature map and voltage drop measurements across different regions of the anode assembly. The results prove a substantial reduction in the overall anode voltage drop, which is primarily attributed to the innovative anode assembly design. This configuration has the potential to decrease the anodic drop voltage by roughly 77 mV, effectively lowering it from 390 mV to 313 mV. This reduction in anodic drop voltage is estimated to translate into annual cost savings of approximately USD 4.6 for a smelter producing 320,000 tons of aluminum annually.

KEYWORDS: Alumina, Hall-Héroult Process, Thermo-Electrical Model, Anode Nails, Anode Voltage Drop, Anode Yoke, Energy Efficiency.

التحديات في توفير الطاقة في خلية استخلاص الألومنيوم عن طريق تحسين تصميم الأنود والإدراجات

عبد المجيد محمد شمروخ[1] ، صلاح عبد الغني سالمان[2]، عمرو بسيونى الديب[2]، محمد كمال جودة[2]، وليم بريندز[3]، وليد عبد الفضيل[4]، جمال تاج عبد الجابر[5]

[1*] شركة مصر للألومنيوم، نجع حمادي، 83642، قنا.

[2] قسم التعدين والبترول، كلية الهندسة، جامعة الأزهر، مدينة نصر، 11884، القاهرة، مصر.

[3] شركة ألوتك، كندا.

[4] قسم التصميم والإنتاج الميكانيكي، كلية هندسة الطاقة، جامعة أسوان، 81542، أسوان ، مصر.

[5] قسم التصميم والإنتاج الميكانيكي، كلية الهندسة، جامعة قنا، 83523، قنا، مصر.

* البريد الاليكتروني للباحث الرئيسي : abdulmajid_business@outlook.com

الملخص

يُنتج الألمنيوم الأولي بشكل أساسي من خلال عملية التحليل الكهربائي Hall-Héroult ، والتي تتميز باستهلاكها الكبير للطاقة. كفاءة الطاقة لهذه العملية هي العقبة الرئيسية التي يواجها منتجو الألومنيوم، والتي لا تتجاوز 50%. في المقابل، يشكل استهلاك الطاقة حوالي 40% من إجمالي تكلفة الإنتاج. يعتبر فرق الجهد عند كل من الأنود والكاثود هو السبب الرئيسي للاستهلاك المفرط للطاقة الكهربائية. ومن الجدير بالذكر أن حوالي 25% من إجمالي فرق الجهد في مجموعة الأنود يحدث عند السطح البيني الصلب/الحديد الزهر/الكربون، بناءً على مقاومة التماس. في هذا العمل، تم تطوير تصميم جديد بنجاح وتم التحقق منه افتراضياً وعملياً باستخدام عدد مختلف من المسامير الصلب و/أو مواقعها. حيث تم تطوير نموذج حراري كهربائي ثلاثي الأبعاد لمجموعة الأنود بواسطة لغة APDL في برنامج .ANSYS ومن ثم تم التحقق من صحة النموذج ثلاثي الأبعاد من خلال إجمالي القياسات لخريطة درجة الحرارة وفرق الجهد عبر مختلف أجزاء مجموعة الأنود. حيث كشفت النتائج التي تم الحصول عليها عن انخفاض كبير في فرق الجهد الكلي للأنود والذي يمكن اعتباره أساسًا للتصميم الجديد لمجموعة الأنود.

الكلمات المفتاحية : الألومينا، التحليل الكهربي، نموذج حراري كهربائي ، مسامير الأنود، فرق الجهد للأنود، الشوكة الأنودية، كفاءة الطاقة.

1. INTRODUCTION

Briefly, the primary production of aluminum consists of dissolving the alumina (Al_2O_3), getting from bauxite by the Bayer process, in molten cryolite (Na_3AlF_6) bath with an excess of aluminum fluoride (AlF_3) and some other additives, all at about 960 ° C. In the presence of a high-intensity electric current, oxygen molecules are liberated from aluminum and swiftly react with carbon molecules existing in the anode, resulting in the generation of carbon dioxide (CO_2). As a result, aluminum agglomerates in liquid form and settles at the bottom of the cathode shell, which has a density higher than that of the bath. Equation (1) represents the chemical reaction activated by the electrolysis process of aluminum [1-7].

$$Al_2O_{3_{Solid}} + 3C_{Solid} \xrightarrow[Electrolysis]{960C^o} 4Al_{Liquid} + CO_{2_{Gas}} \rightarrow (1)$$

($E_{Reversible}$ =1.22 V at 960◦C) [8]

Aluminium is a non-ferrous metal that is widely used today. Its applications have a very wide range from transportation to backing, construction, electrical power lines, household items, and more. However, its presence in everyday life is relatively new[9].

In an aluminum smelter, the reduction cells - also called “pots” - have aligned in series end-to-end or side-by-side and the total number of cells varies according to the smelters. Nonetheless, there are various cell technologies that are available worldwide. In the current study, the numerical model was developed based on the AP-21 cell technology, pioneered by the Pechiney group and now employed by Rio Tinto-Alcan. This choice has made considering that this technology is exclusively used at the Aluminium Company of Egypt (Egyptalum) smelter. These cells have been reported to run at around 210 KA.

Due to the fact that power consumption constitutes approximately 40% of the overall production cost, the declining trend in London Metal Exchange (LME) aluminum prices, coupled with the rising cost of energy, has prompted aluminum producers worldwide to prioritize energy conservation efforts [10]. A promising solution for minimizing energy losses and, so, production costs involve the reduction of electrical resistance at the stub-to-carbon interface within the anode assembly.

Consistent with the research conducted by Alexander Arkhipov et al., the design and assembly of anode components in aluminum reduction cells exert a significant influence on both cell voltage and heat loss [9]. Literature shows that upon trimming of cast-iron to eliminate the gap between the steel stub and carbon block, the solidifying cast-iron thimble becomes firmly attached to the anode stub hole and steel stub surfaces. During the initial phases of crystallization and solidification, the cast-iron undergoes a volume contraction, leading to a snug fit of the cast-iron thimble on the stubs [12, 13]. The thermal shrinkage of iron results in an initial air gap between the cast-iron thimble and the carbon stub-hole wall, causing low contact pressure between them. [14-

16]. The volume of the air gap at this region after cooling to normal working temperature is governed by the cast-iron thickness. The solidification shrinkage influenced by various factors just like the cast-iron chemistry, the carbon content, and also the cooling rate [17].

About the quarter of voltage drop of the anode assembly is up to the steel/cast iron/carbon interfaces [1], The existence of an air gap within the anode assembly, when installed in the cell, can have a detrimental impact on its energy efficiency [18], An excessively large air gap can give rise to high resistance and ohmic heating, consequently resulting in substantial energy consumption at the stub/carbon interface. Conversely, a certain degree of air gap is essential to compensate for the thermal expansion of the steel stub, which exhibits a coefficient of thermal expansion (CTE) approximately three times that of carbon [19], Completely eliminating the air gap could lead to excessive stress within the anode, potentially leading to cracking.

As a result of metal creep at the final stages of anode operation, slow self-forging phenomena have appeared on steel stubs during each anode cycle. The extreme thermal environment surrounding the steel stub, coupled with the expansive pressure exerted by the steel stub against the restrictive force of the stub hole, leads to a self-forging behavior that is irreversible. This phenomenon, in conjunction with potential surface corrosion from the molten bath, has resulted in a gradual reduction in the stub diameters over time.

The magnitude of the air gap is primarily determined by several factors, namely i) the temperature of the molten iron during pouring, ii) the temperature of the carbon and steel stub during the solidification of the cast iron, iii) the chemical composition of the cast iron, and iv) the thickness of the cast-iron itself [2]. Given that the air gap introduces substantial contact resistance at the stub-to-carbon interface, its minimization is essential for enhancing anode performance [20]. **Fig. 1** depicts the presence of an air gap and a crack within the cast-iron thimble.

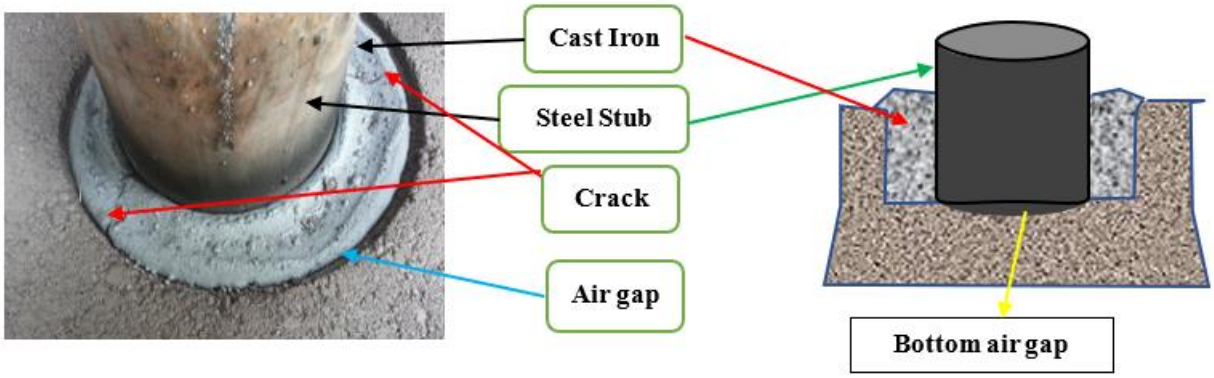

Fig. 1. The real in-situ and the schematic of cracks and the air gap in the cast-iron surrounded steel stub.

In 1976, Peterson equipped and worked on an anode assembly with (30) voltage probes and (50) thermocouples to enable continuous monitoring of temperature and potential readings. Peterson identified the contact interfaces at the stub-to-carbon region as being influenced by temperature and estimated that these interfaces contributed to about 25% of the overall anode voltage drop. Despite encountering difficulties in evaluating the electrical contact resistance between cast-iron and carbon, Peterson observed a decrease in stub-carbon resistance as the stubs were heated, reaching a minimum value of around 600°C [14]. Two years later, Peterson revisited the influence of varying cast-iron volume in the stub-hole region on temperature by repeating these experiments with a modified stub-hole design and placing the assembly in an oven. While still unable to precisely determine the electrical contact resistance at the cast iron/carbon interface, Peterson noted that elevating the temperature appeared to reduce the resistance to negligible levels [21].

Building upon Peterson's work, Brooks and Bullough in 1984 delved into the impact of cast-iron thickness on electrical contact, aiming to optimize cast-iron thickness. Their investigations

revealed a considerable influence of both temperature and contact pressure on contact resistance. This led them to propose design charts for cylindrical connectors [22].

In the early 1990s, Sørlie and Gran introduced a tool for measuring the electrical contact resistance (ECR) of cathode material [23]. Their tool demonstrated a strong influence of both temperature and pressure on ECR. They concluded that a significant reduction in ECR was a function of normal pressure, reaching a plateau at approximately 2 MPa.

In the same year, Mark Dupuis et al.[24] examined the impact of cast-iron thickness on 24 commercial anode connections with varying stub diameters. Their goal was to figure out the best cast-iron thickness and casting conditions that would minimize anode cracking and stub operating temperatures while maintaining a low-resistance stub-carbon connection. They established that the ECR decreased and then leveled off as the stub temperature increased, indicating the tightness of the connection. Based on their findings, they developed charts for the best cast-iron thickness, yielding equivalent results.

Between 2000 and 2003, Richard et al. replicated the experiment conducted by Sørlie and Gran [23] using anode material [25]. Based on their experimental data results, they proposed a constitutive law expressed in the form of the Weibull equation, which was validated against data published by Brooks and Bullough [22].

In 2014, W. Berends filed a patent for the insertion of anode nails into the stub hole [26, 27]. The nails function as electrical conductors across the shrinkage gap between the cast-iron and stub hole wall, reducing power consumption over the entire anode life through reduced electrical contact resistance and improving current distribution throughout the anode. The nails are composed of carbon/steel and remain attached to the thimble during recycling, becoming part of the remelted cast-iron for subsequent rodding. **Fig. 2** illustrates the potential positioning of nails in the anode assemblies.

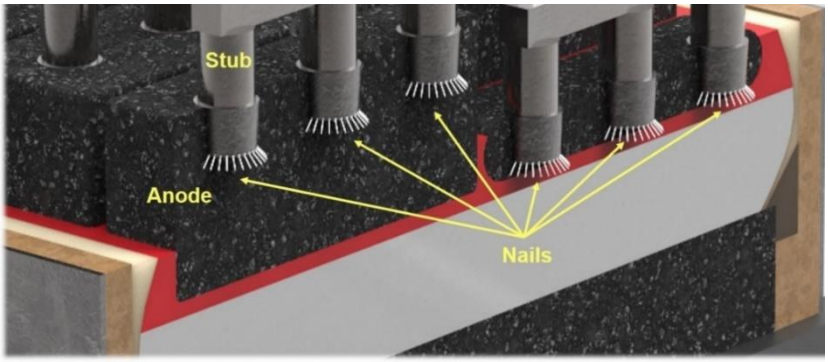

Fig. 2. Illustrates the placement of anode nails within an anode assembly. (Source AluCellTech)

This research addresses this critical gap by investigating the effectiveness of introducing steel nails into the stub hole of anode blocks to minimize the overall voltage drop. By strategically placing nails in the bottom and/or sidewalls, we aim to influence the Thermo-Electro-Mechanical (TEM) interplay within the anode. The temperature rise due to operation will induce thermal expansion of materials, potentially improving contact pressure and current transmission through the following mechanisms:

- Reduced electrical contact resistance: Nails provide additional conductive pathways, bypassing potential high-resistance regions in the cast iron.
- Enhanced displacement and mechanical contact: Nails function as anchors, preventing relative movement between the thimble and stub, ensuring consistent contact.
- Improved thermal conductance: Direct contact between nails and surrounding carbon/cast facilitates efficient heat transfer, potentially reducing hot spots and Joule heat generation.

This investigation will offer valuable insights into optimizing anode design and performance, potentially leading to reduced energy consumption and enhanced efficiency in aluminum production.

Four case studies were investigated in the industrial field. These cases include the effect of the locations and the number of inserted nails. The obtained results demonstrations that there is a remarkable reduction in the total voltage drop of anode assembly by inserting steel nails from traditional anode assembly without nail and the reduction value is affected by the quantity of inserting nails. The proposed design incorporates twelve steel nails at the bottom and an additional six nails along the sidewall of the stub hole. This configuration has the potential to decrease the anodic drop voltage by roughly 77 mV, effectively lowering it from 390 mV to 313 mV. This reduction in anodic drop voltage is estimated to translate into annual cost savings of approximately USD 4.6 for a smelter producing 320,000 tons of aluminum annually.

2. Materials and Methods

2.1 Anode Nails insertion

To mitigate the impact of air gap occurrence at the STC interface after solidification of cast-iron thimble, a series of experiments have been functioned. In the first test, six steel nails were inserted in the bottom of the stub hole.

To enhance the connection between cast-iron and carbon block, and then reduce the connection resistance, five trials were conducted. The first trial serves as the baseline, with no modifications to the anode carbon block, as depicted in **Fig. 3A**. In the next trial, six 5-mm-diameter nails were inserted into pre-drilled holes at the bottom of the stub hole, as illustrated in **Fig. 3B**. The third trial explores the impact of nail placement by inserting six 5-mm-diameter nails into pre-drilled holes along the sidewall of the stub hole, as shown in **Fig. 3C**. The fourth trial examines the effect of nail quantity by inserting twelve 5-mm-diameter nails into pre-drilled holes at the bottom of the stub hole, as illustrated in **Fig. 3D**. Finally, the fifth trial further investigates the influence of nail quantity by inserting twelve 5-mm-diameter nails into pre-drilled holes at the bottom of the stub hole, as depicted in **Fig. 3E**.

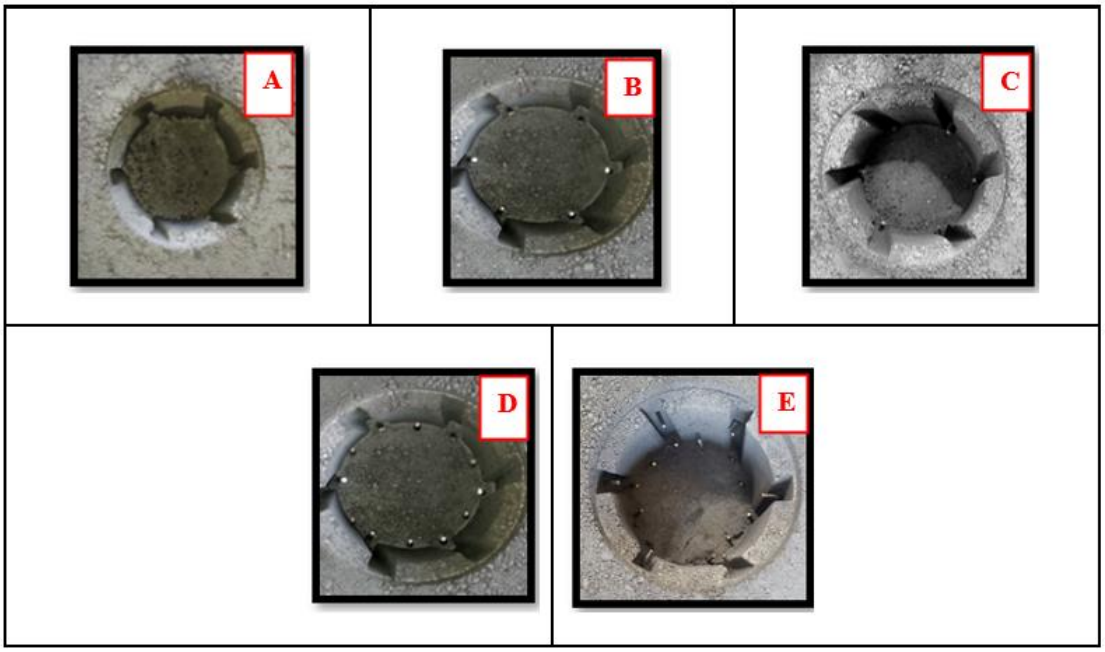

Fig. 3. Trials case on Nails inserting, where (A) without nails, (B) 6-nails at bottom, (C) 6-nails at sidewall, (D) 12-nails at bottom and (E) 18-nails at bottom.

2.2 Thermal Measurements

The temperature measurements on stubs, steel yoke, and the aluminium rod in addition to the temperatures that are recognized by inserted thermocouples in cast-iron collars and carbon block, are recorded for the base case anode block tests without nails insertion, and the other four experiments contain steel nails with different quantities and at different locations are recorded.

2.3 Voltage Drop Measurements

The voltage measurements were done at various locations between specific points. The algebraic sum of these individual measurements is the total voltage drop over the anode assembly.

2.4 FE Model

2.4.1 Model Development

The first step involved creating a comprehensive model of the anode assembly within the Autodesk Inventor® program. Subsequently, this assembly was imported into ANSYS Workbench® to construct a model using the APDL language (ANSYS® Parametric Design Language). In ANSYS®, the automated process facilitated seamless connections between dissimilar bodies through the application of CONTA174-TARGE170 contact elements, encompassing temperature, structural, and electrical degrees of freedom, as detailed elsewhere [12].

The pivotal factor for achieving a validated model and favorable outcomes lay in accurately specifying material properties and boundary conditions. Essential physical properties influencing the stub-anode connection included thermal expansion, electrical resistivity, and thermal conductivity, as documented in existing literature. Notably, an adiabatic boundary condition was applied in this model to assess the impact of the anode cover, not explicitly accounted for, on insulating the upper section of the carbon block and stubs.

By using the Laplace equation to define the voltage drop through the Anode carbon block at a definite condition:

$$\nabla^2 V = 0 \rightarrow (2)$$

Where V is the voltage drop, by using Cartesian coordinates where in the 2D system the anode carbon block considers as cuboid as illustrated in **Fig. 4**.

$$\nabla^2 = \frac{\partial^2}{\partial x^2} + \frac{\partial^2}{\partial y^2} + \frac{\partial^2}{\partial z^2} \rightarrow (3)$$

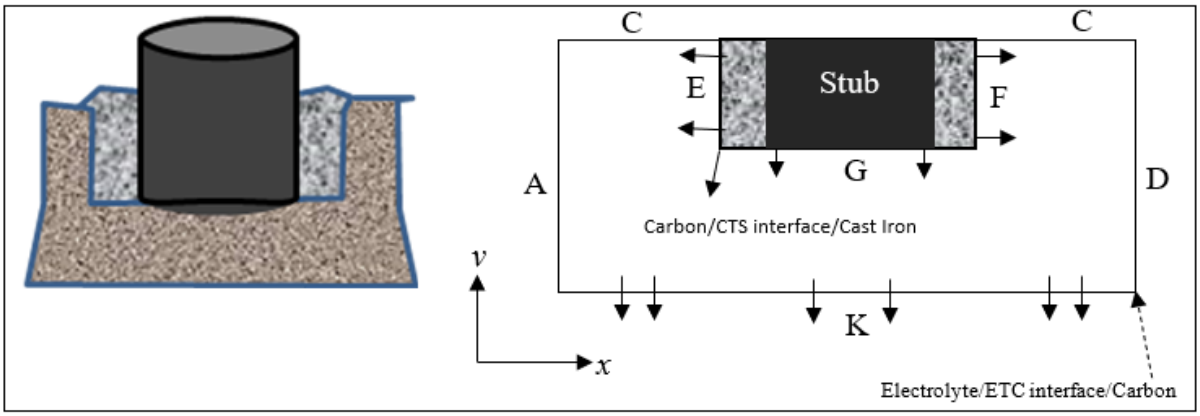

Fig. 4. Anode Carbon Block Slice.

Where the current (I) goes through the interfacial regions perpendicularly, then the voltage drop at E, F and G regions could be calculated using Ohm's law.

$$\Delta V = I\left(\frac{\rho\lambda}{A}\right) \rightarrow (4)$$

Where: A is the contact interface area, ρ is the specific resistance of the interfacial surface, and λ is the thickness of the interfacial surface.

Practically each interface is considered as a very thin film, so it's not possible to measure ρ and λ for it dependably. Based on this fact the physical quantity ρλ was constituted with another quantity CR which represent the contact resistance. There are significantly published papers to measure and predict the value of CR, Richard et al., proved the almost accepted formula to predict this value. They reported that the optimum pressure value to ensure a good contact between the carbon and cast-iron is equal to 6.2×10^7 Dyne/cm^2, and this value will achieve a good contact resistance equal 2.32×10^{-2} Ω.cm^2[12].

To highlight the model's predictive power, a conventional anode design without nail insertion has been simulated in the initial phase. Subsequently, the novel anode design with various nail insertion scenarios, encompassing different nail quantities and locations, was simulated in the second phase. The smelter considered the stub and cast-iron conditions in the tests to be 'typical'. The analysis of measured data elucidated the influence of steel nails on the performance of the anodes.

2.4.2 Loads and Boundary Conditions

At the Egyptalum smelter, a substantial working current of 210 KA/Pot-Room caused the application of an electrical current of 8750A on each aluminum rod within the anode assembly, with this assumed voltage located at the bottom surface of the anode block equal zero. Notably, the numerical simulation excluded consideration of the bath. To mimic the anode immersion, a convective flux was implemented at the anode's base, extending to a depth of 150 mm. This involved a convection coefficient set at 500 W/m2 °C, with an ambient temperature of 960 °C factored in for the corresponding flux[12, 27, 28]. It's crucial to highlight the omission of periodicity conditions between central and outer anodes in the cell, and the heat fluxes on the lateral sides of the anode were intentionally neglected in the simulation.

The voltage drop at region K (the bottom surface of the anode) can be calculated using the equation:

$$V_K = V_{Anode} - (V_{E,F,G} + V_{stub}) \rightarrow (5)$$

It's clear V_K is equal zero, then:

$$V_{Anode} = (V_{E,F,G} + V_{stub}) \rightarrow (6)$$

2.4.3 Model Validation

It's worth noting that there is a slight variance between the numerical model and the real operating reduction cells, because of the un-continuity stability of operating conditions. It's likely to note the diameter of steel stub is not constant, but it decreases continuously because of degradation, and consequently the size of the cast-iron thimble is increased. The operating temperature in aluminium reduction cells isn't stable, but it could changeable according to operating parameters, but it must maintain in closed range. The composition of cast-iron also may be changed in each patch, all the earlier discrepancy in the operating conditions may cause a significant impact on the field measurements. By comparing the obtained values of temperature from the thermal model with its corresponding measurements, it has negligibly variance. Another validation evidence has been realized by comparing the recorded voltage drop measurements, between specified points over the anode assembly in operating reduction cells with the prediction values from numerical model over the same points. The voltage drop obtained from Ansys model equals 348 mv. Whereas the in-situ measured is 370 mV, this means the difference is about 6%. The obtained variance percent is a very good covenant with else published date, which decide that the satisfactory variance is ranging from 2-13% [24].

3. RESULTS AND DISCUSSION

Voltage Drop Measurements

In Base Case: As illustrated in **Fig. 5**, it's clear that the voltage drop measurement over the cast-iron thimbles is convergent and falls in the range (151 – 390 mv) through the anode life cycle.

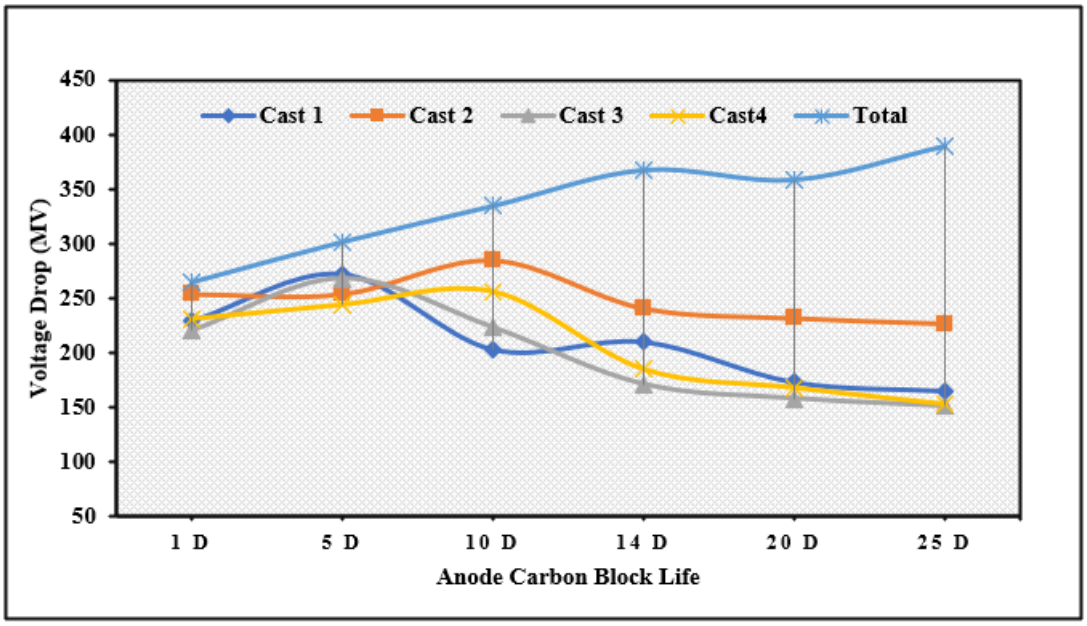

Fig. 5. Voltage drop measurements (millivolts) of reference base Case.

In the case of inserting 6 nails at the bottom of the stub hole: The voltage drop measurement over the cast-iron thimbles is convergent and falls in range (141 – 370 mv) through the anode life cycle, this means we can save about 20 mV through applying this trail as shown in **Fig. (6-a)**.

In the case of inserting 6 nails at the sidewall of the stub hole: The voltage drop measurement over the cast-iron thimbles is convergent and falls in range (123 – 373 mv) through the anode life cycle, this means we can save about 17 mV through applying this trail as shown in **Fig. (6-b)**.

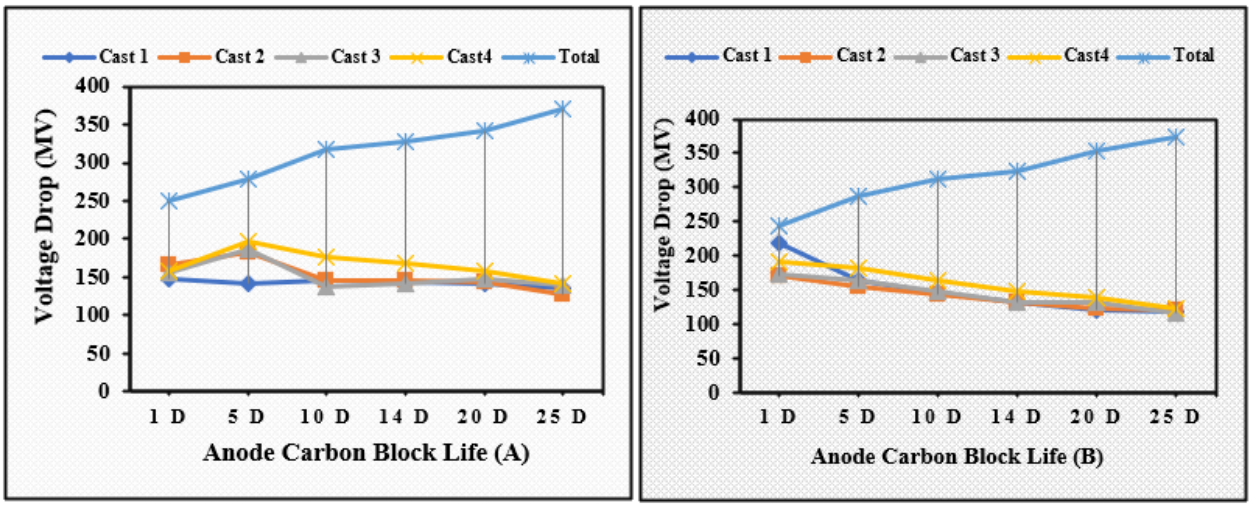

Fig. 6. Voltage drop measurements of trial No 2 (A) & 3 (B).

The predicted value of voltage drop over total anode assembly through finite element model that has been developed by adding a six steel nails at the bottom or at the side wall of the stub-hole as shown in **Fig. 7**, also agrees with these corresponding values that are predicted from numerical model by an acceptable variance.

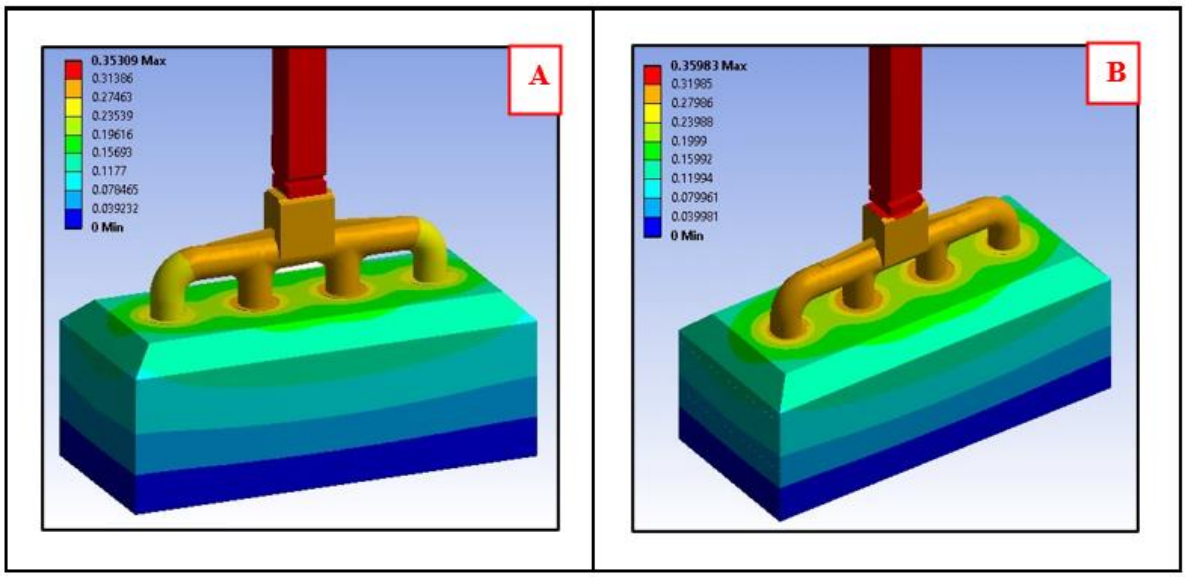

Fig. 7. The predicted voltage drop values over the experimental No. 2 & 3, where A) Six nails inserted at the bottom of the stub-hole and B) Six nails inserted at the side wall of the stub-hole.

In the case of inserting 12 nails at the bottom of the stub hole: The voltage drop measurement over cast-iron thimbles is convergent and falls in the range (104 – 324 mv) through the anode life cycle, this means we can save about 66 mV through applying this trail, it's clear the number of the inserting nails has a strong influence on the achievable saving amount as shown in **Fig. (8-a)**. In the case of inserting 12 nails at the bottom of the stub hole further to 6 nails at sidewall: The voltage drop measurement over cast-iron thimbles is convergent and falls in range (73 – 305 mv) through the anode life cycle, this means we can save about 85 mV through applying this trail, it's clear the coupling of quantity and location of the inserting nails has a strong impact on the achievable saving amount in total voltage drop **Fig. (8-B).**

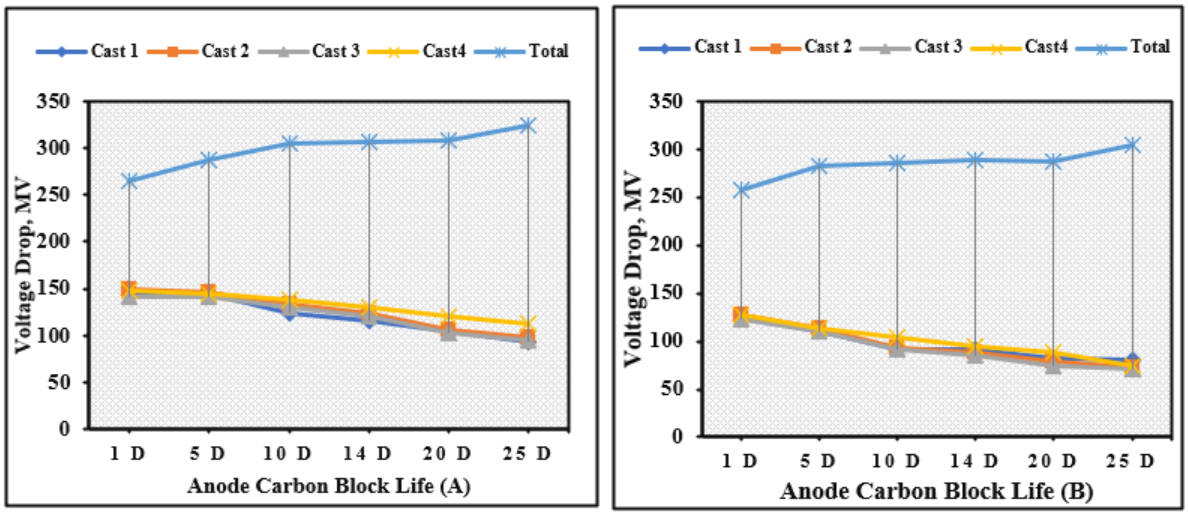

Fig. 8. Voltage drop measurements of trial No 4 (A) & 5 (B).

By comparing the measured total voltage drop value of in-situ anode assembly with this corresponding value of the numerical model as depicted in **Fig. 9**, it's differed by an adequate value (2.5%). The obtained difference value is considered as evidence to ensure the model's validity and reliability.

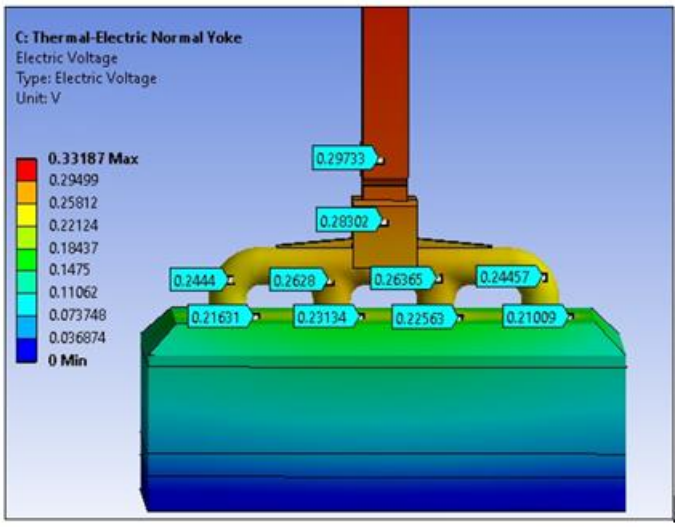

Fig. 9. The predicted voltage drop values over experimental No. 5.

The reachable amount of saving in case of inserting six steel nails at the bottom or at the sidewall of the stub-hole (20 & 17 mV) is less than the half of reachable amount by inserting twelve steel nails (66 mV), while the sum of reachable amount in two cases together is less than that achievable in the current case (85 mV). **Fig. 10** recapitulates the obtained results through whole experiments.

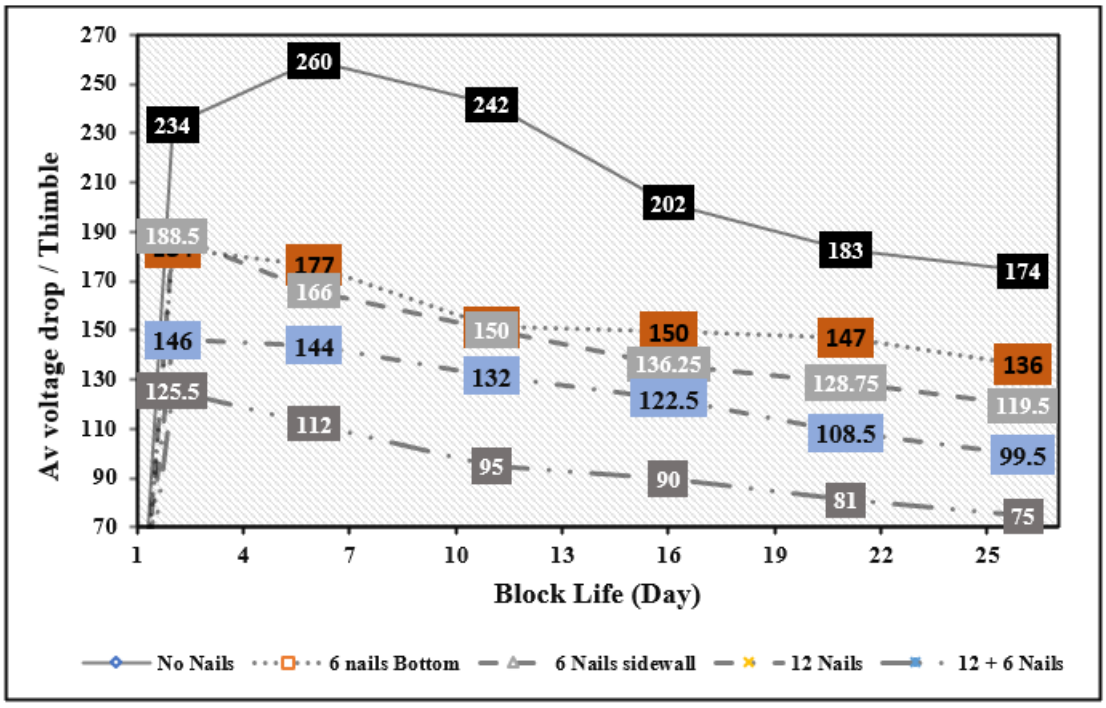

Fig. 10. The average voltage drop measured over each cast-iron thimble during anode carbon block life.

It is clear from the earlier figures that inserting nails directly affects the average voltage drop for each cast-iron thimble over the entire carbon block life. The nail insertion method has an impact not only on both the voltage drop value and the time needed to pick up the new anode carbon block, but addition also to make fluctuations of changing in voltage drop more smoothly over anode block life. **Fig. 11** summarizes the obtained results through whole experiments.

The number and placement of inserted nails exert a substantial influence on the attainable savings in terms of the total voltage drop. The overall cost incurred by inserting nails at the bottom

and sidewall of the stub hole totals 370,700 USD/yr. In contrast, the total income gained by inserting nails at the bottom and sidewall of the stub hole amounts to 4,921,449 USD/yr. The net annual potential cost saving, calculated based on a voltage drop reduction of 75 mV per anode block, is estimated to be 4,550,749 USD/yr. [28].

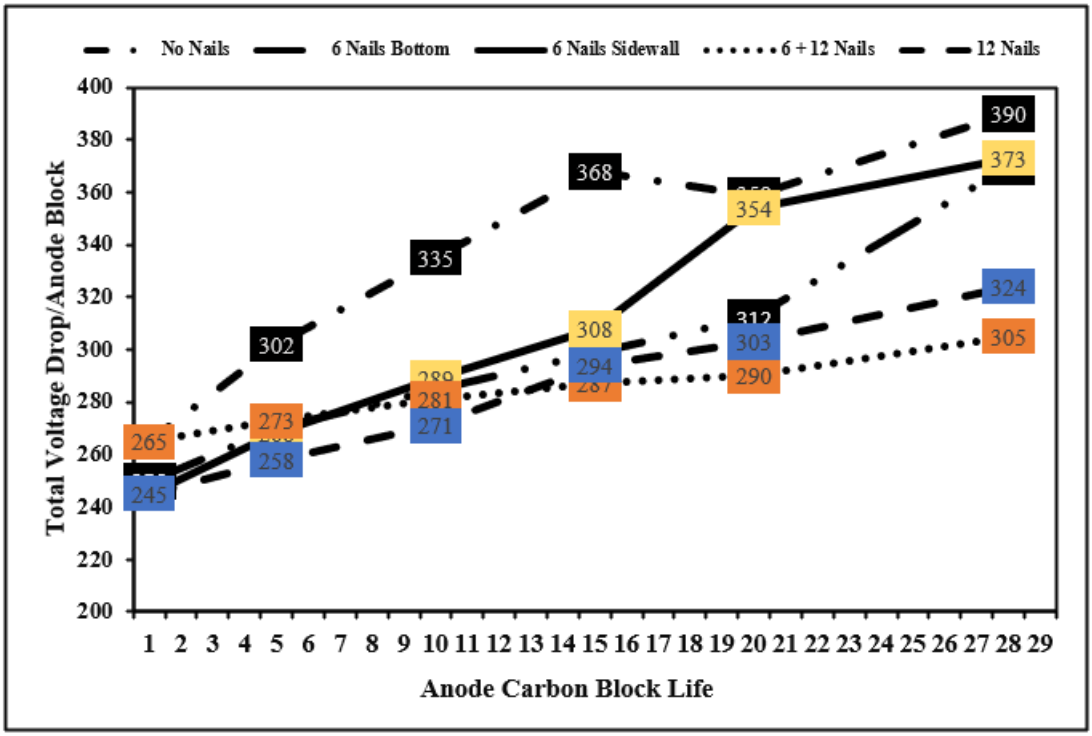

Fig. 11. The average voltage drop measured over each cast-iron thimble during anode carbon block life.

Conclusions and Recommendations:-

To simulate the effect of inserting nails on the total gained voltage drop, a set of numerical models (3D thermo-electrical-mechanical) of total anode assembly was developed using APDL ANSYS® software. The current anode assembly is represented by the base model without nails. The simulations, coupled with in-situ experiments at the Egyptalum smelter, demonstrated a significant reduction in total anode voltage drop due to the innovative nail configuration.

The obtained results display in clear an acceptable agreement of temperature and voltage distribution has been achieved with strong impact of inserting nails of the total voltage drop of anode assembly. By applying the fourth technique described previously, it will supply a net annual potential cost savings of 75 mV/anode block, which equals USD 4,550,749 per year.

The innovative anode assembly design has the potential to significantly reduce energy consumption and production costs in the aluminum industry. Furthermore, the principles underlying our approach could potentially be applied to other sectors that rely on electrical processes with high energy demands.

The limitations of our study: The authors acknowledge that while the experimental results are promising, further research is needed to fully understand the long-term effects of nail insertion on anode assembly performance and to evaluate its applicability in whole industrial scale. Additionally, while our numerical model provides valuable insights, it is important to note that it is based on certain assumptions and simplifications related to the current physical and chemical composition of the anode assembly materials.

- Scaling Up: Based on our promising findings, we propose scaling up the experiment to the entire reduction cell to assess the overall reduction improvement. This will supply a crucial validation of the technology's potential impact on industrial-scale operations.

- Optimization Through Parameter Exploration: We recommend further investigating the influence of nail parameters on performance by varying the number, length, diameter, and location of the inserted nails. This systematic exploration will optimize nail configuration for maximum reduction efficiency.
- Automation for Efficiency: To facilitate faster and more precise nail insertion, we suggest exploring the use of robotic arm technology. This automation has the potential to significantly reduce labor costs and improve experiment consistency.
- Mitigating Stub Diameter Reduction: We further propose studying the effectiveness of nail inserts in compensating for the reduction in stub diameter caused by attrition. This investigation could pave the way for extending the lifespan of anode components and reducing maintenance costs.

References

1. Ebrahim Jeddi, Daniel Marceau, Laszlo L Kiss, Lyne St-Georges, Denis Laroche and Lyes Hacini, "Experimental and numerical investigation of voltage drop in anode assemblies", in TMS (The Minerals, Metals & Materials Society), 2013, B. Sadler, Editor. 2013, Springer: US. p. 1347-1352.
2. Ebrahim Jeddi, "Numerical study of anodic voltage drop in the Hall-Héroult cells by finite element method". 2013, Qubec University.
3. ElDeeb A.B., Brichkin V.N., Sizyakov V.M., Kurtenkov R.V., 2020. Effect of sintering temperature on the alumina extraction from kaolin. Pp. 136–145 in: Advances in Raw Material Industries for Sustainable Development Goals (E. Litvinenko, editor). CRC Press, Boca Raton, FL, USA.
4. ElDeeb A.B., Brichkin, V.N., Kurtenkov R.V., Bormotov I.S., 2019. Factors affecting on the extraction of alumina from kaolin ore using lime-sinter process. Pp. 502-508 in: Topical Issues of Rational Use of Natural Resources 2 (E. Litvinenko, editor). CRC Press, Boca Raton, FL, USA.
5. ElDeeb A.B., Brichkin V.N., Bertau M., Awad M.E., Savinova Y.A., 2022. Enhanced alumina extraction from kaolin by thermochemical activation using charcoal. Clay Minerals 56(4), 269–283.
6. ElDeeb A.B., Brichkin V.N., Povarov V.G., Kurtenkov R.V. 2020. The activating effect of carbon during sintering the limestone-kaolin mixture. Tsvetnye Metally 7: 18-25.
7. ElDeeb A.B., Brichkin V.N., Kurtenkov R.V., Bormotov I.S., 2021. Study of the peculiarities of the leaching process for self-crumbling limestone–kaolin cakes. Obogashchenie Rud, 2021, 27–32.
8. Jessen, S.W., "Mathematical modeling of a Hall Héroult aluminum reduction cell". 2008, Technical University of Denmark.
9. Peng Jianping, Di Yuezhong, Wang Yaowu and Feng Naixiang, "Increasing the Energy Efficiency of Aluminum-Reduction Cells Using Modified Cathodes. JOM : Journal of The Minerals, Metals & Materials Society, 2017. 69: p. 1767–1772.
10. Amit Gupta and et al., "Impact of copper insert on low amperage aluminium reduction cell", International Conference and Exhibition of ICSOBA, Dubi, 2015.
11. Alexandre Arkhipov and et al, "Review of Thermal and Electrical Modelling and Validation Approaches for Anode Design in Aluminium Reduction Cells", in Proceedings of the 36th International ICSOBA Conference, . 2018: Belem, Brazil. p. 589-607.
12. Hugues Fortin and et al, "FEM analysis of voltage drop in the anode connector induced by steel stub diameter reduction", Elsevier 2012. 52: p. 71-82.
13. Hugues Fortin and et al, "Thermo-electro-mechanical characterization of anode interfaces at operating conditions", in TMS (The Minerals, Metals & Materials Society), B. Sadler, Editor. 2013: US. p. 1335-1340.

14. Gran and et al, "Property changes of cathode lining materials during cell operation", in Light Metals: TMS (The Minerals, Metals & Materials Society), J.W. Evans Editor. 2013: US. p. 936-941.
15. Daniel Richarda and et al, " Carbon to cast-iron electrical contact resistance constitutive model for finite element analysis", Journal of Materials Processing Technology, Vol. 192, p. 119-131.
16. Ayoola Brimmo and Mohamed I. Hassan, "Modeling the Electrical Contact Resistance at Steel–Carbon Interfaces". JOM: the journal of the Minerals, Metals & Materials Society · 2016. 68: p. 49-58. JOM: the journal of the Minerals, Metals & Materials Society, 2015. 68(1, 2016): p. 49-61.
17. Richard w. Peterson, "Studies of stub to carbon voltage. Electrode technology for aluminum production", 1978. 4: p. 510-515.
18. Susann Beier, "A study of an anode assembly with focus on the anode connection used in aluminium reduction cells", PhD Thesis, 2010, Auckland university.
19. Bullough and et al al, "Factors in the design of reduction cell anodes", in TMS (The Minerals, Metals & Materials Society). 1984. p. 516-523.
20. Yang Sun, K.G.F., Morten Sørlie and H. A. Øye, "3D Modelling of thermal and sodium expansion in Soderberg aluminium reduction cells", in in Light Metals: TMS (The Minerals, Metals & Materials Society). 2004: US.
21. Ayoola Brimmo and et al, " Anode design modeling for improved energy efficiency", International Conference and Exhibition of ICSOBA, Dubi, 2015.
22. D. Richard, R. Lacroix, P. Clery, and Y. Maltais, "Aluminum reduction cell anode stub hole design using weakly coupled thermo-electro-mechanical finite element models". Finite elements in analysis and design. 2001. p. 287-304.
23. Richard W. Peterson and et al al, "Anode cast-iron thickness optimization", in Light Metals: TMS (The Minerals, Metals & Materials Society). 1990. p. 524-528.
24. Daniel Marceau and et al, "Experimental and Numerical Investigation of Voltage Drop in Anode Assemblies", in TMS (The Minerals, Metals & Materials Society), B. Sadler, Editor. 2015: US. p. 1347-1352.
25. Susann Beier, J.C., Hugues Fortin and Mario Fafard, " FEM analysis of the anode connection in aluminium reduction cells", in TMS (The Minerals, Metals & Materials Society), 2011: US. p. 979-984.
26. William Berends, "The Impact of Anode Nails on the Stub to Carbon Electrical Contact Resistance of Anode Assemblies with Simulated Corroded Stubs", in TMS (The Minerals, Metals & Materials Society), A.P. Ratvik, Editor. 2017: US. p. 1341-1347.
27. William Berends, "Low resistance electrode assemblies for production of metals". Canadian Intellectual Property Office: Canda, 2014: p. 1-74.
28. Abdul-Majid Shmroukh, Sa. Salman, Will Berends, W. Abdel Fadeel and G. Tag Abdel Gabr, "Energy Saving in Hall–Héroult Cell by Optimization of Anode Assembly Design", in TMS (The Minerals, Metals & Materials Society), A.P. Ratvik, Editor. 2020: US. DOI: 10.1007/978-3-030-36408-3_174.